Ocean Engineering 37 (2010) 252–261

Contents lists available at ScienceDirect

Ocean Engineering

journal homepage: www.elsevier.com/locate/oceaneng

Hydroelastic analysis of the floating plate optimized for maximum radiation damping

Christopher J. Damaren *

University of Toronto, Institute for Aerospace Studies, 4925 Dufferin Street, Toronto, Ontario, Canada M3H 5T6

ARTICLE INFO

Article history:
Received 30 June 2009
Accepted 25 October 2009
Available online 31 October 2009

Keywords:
Hydroelasticity
Floating plates
Shape optimization

ABSTRACT

In previous work, the problem of optimizing the shape of a thin floating plate to maximize radiation damping was investigated. The plate was modelled with zero draft and floated on the surface of an irrotational, incompressible ocean of infinite extent. For simplicity, only rigid heave motions were considered and the damping coefficient at one wave number was maximized. In the present work, the hydroelastic properties of the optimized plate are determined and compared with those of circular and square plates. The added mass, damping, and diffraction force coefficients in each mode are determined as a function of wave number. The amplitude responses of the plate deflection and bending moments are also presented. The finite element method is used to determine the vibration mode shapes and the flow problem is analysed using the Chen and Mei variational principle wherein the potential field inside a hemisphere surrounding the plate is represented using a spherical harmonic expansion and matched on the hemisphere to an outer field described by distributing sources on the hemisphere.

1. Introduction

For very large floating structures (VLFS), structural flexibility becomes important and one must describe its interaction with the fluid motion. In many applications, it is desirable that the motions of the structure be suppressed given excitations stemming from external loads and wave forces. Like the rigid body case, one may construct frequency responses relating the external forcings to the amplitude of the modal coordinates. The amplitude decay of transient responses is a strong function of the frequency-dependent damping coefficients. These coefficients result from the radiated waves produced by structural motions which result in a net transfer of energy away from the structure.

An important class of VLFS are thin plates such as floating airports where the mat-like structure resides in the free surface. The hydroelasticity of this type of structure has been considered by Andrianov and Hermans (2005) and Watanabe et al. (2006) for circular plates while Damaren (2001) has studied the rectangular case. A survey of work in this area has been done by Watanabe et al. (2004). Earlier work by Ertekin and Kim (1999) examined responses of thin plates to oblique, shallow-water waves. Recently, Xia et al. (2008) looked at the responses of a two-dimensional VLFS to solitary waves such as a tsunami wave. Riggs et al. (2008) have compared hydroelastic computer codes using a VLFS benchmark problem.

Suppression of the vertical motions of these structures requires appropriate sources of energy dissipation. These include structural damping (including both material effects and those due to articulations such as joints), viscous fluid effects, and radiation damping due to the production of outgoing surface waves. In previous work (Damaren, 2007), we were concerned with the desire to optimize the planform shape of a thin floating plate to maximize the radiation damping effect. It is expected that radiation damping will dominate over the other two effects in applications. In that work, only rigid-body heave motion was considered and the damping coefficient at one wave number was maximized. The present paper seeks to examine the hydroelastic properties of the optimal shape determined in the former paper. In particular, we present the added mass, damping, and diffraction force coefficients over a range of wave numbers for the optimal plate as well as circular and square plates. In addition, the plate deflection and bending moments are also presented for the three plate shapes.

The plate is assumed to float on the free surface of an inviscid, incompressible, and irrotational ocean of infinite depth. The potential flow problem is solved using the variational principle developed by Chen and Mei (1974) and detailed by Mei (1989). The inner field within a hemisphere encompassing the plate is described using a spherical harmonic expansion. The outer field is described by distributing sources on the exterior of the hemisphere and it along with its normal derivative is matched to those

* Tel.: +1 416 667 7704; fax: +1 416 667 7799.
E-mail address: damaren@utias.utoronto.ca

0029-8018/$ - see front matter © 2009 Elsevier Ltd. All rights reserved.
doi:10.1016/j.oceaneng.2009.10.008

of the inner field using the variational principle. The vibration modeshapes of the flexible plate are determined using the finite element method with triangular shape elements used to capture the irregular shape of the optimal plate.

2. Hydroelastic boundary value problem

Consider the vertical motion of a thin floating plate which is structurally flexible and lies in the free surface of an irrotational, incompressible ocean of infinite depth. The plate is assumed to be homogeneous and isotropic. We use a coordinate system $\mathbf{r}=[x\ y\ z]^T$ where the plane $z=0$ corresponds to the mean free surface and the $z-$axis is vertically upward. The origin corresponds to the geometric centre of the plate which we also assume is the mass centre given a homogeneous mass distribution. The wetted surface of the plate is denoted by B and the undisturbed free surface is designated F which is the surface $z=0$ less the plate surface B. The undisturbed fluid occupies V which is the half-space $z\le 0$ less the plate surface B. It is assumed to be bounded by a cylinder S_∞ whose radius tends to infinity and whose bottom B_∞ tends towards infinite depth (see Fig. 1).

The vertical motion of the plate is given by $w(x,y,t)$ and the equation of motion is given by

$$\sigma\ddot{w}(x,y,t)+D\nabla^4 w(x,y,t)=p(x,y,t) \tag{1}$$

where σ is the constant mass density per unit area, D the plate rigidity, ∇^4 the biharmonic operator, and $p(x,y,t)$ the hydrodynamic pressure. The boundary of the plate will be described using polar coordinates $r(\chi)$ (see Fig. 2). The direction of the outward normal to the plate edge will be denoted by n and t is the direction of the tangent to the edge. The angle between the outward normal and the x-axis is denoted by θ.

On the edge of the plate, the following (natural) boundary conditions hold:

$$M_n=0,\quad Q_n+\frac{\partial M_{nt}}{\partial t}=0 \tag{2}$$

where

$$M_n=M_x\cos^2\theta+2M_{xy}\cos\theta\sin\theta+M_y\sin^2\theta$$

$$M_{nt}=(M_y-M_x)\cos\theta\sin\theta+M_{xy}(\cos^2\theta-\sin^2\theta)$$

$$Q_n=Q_x\cos\theta+Q_y\sin\theta$$

and

$$M_x(x,y,t)=-D\left(\frac{\partial^2 w}{\partial x^2}+\nu\frac{\partial^2 w}{\partial y^2}\right),\quad M_y(x,y,t)=-D\left(\frac{\partial^2 w}{\partial y^2}+\nu\frac{\partial^2 w}{\partial x^2}\right)$$

$$M_{xy}(x,y,t)=-(1-\nu)D\frac{\partial^2 w}{\partial x\partial y},\quad Q_x(x,y,t)=\frac{\partial M_x}{\partial x}+\frac{\partial M_{xy}}{\partial y},$$

$$Q_y(x,y,t)=\frac{\partial M_{xy}}{\partial x}+\frac{\partial M_y}{\partial y} \tag{3}$$

Here, ν is Poisson's ratio, M_x and M_y are bending moments (per unit length), M_{xy} is the twisting moment (per unit length), and Q_x and Q_y are vertical shearing forces (per unit length). Note that Eq. (2) expresses an absence of bending moment and shear resultant on the free edge of the plate.

The natural modes of vibration correspond to solutions of the unforced problem ($p(x,y,t)=0$) of the form

$$w(x,y,t)=\mathrm{Re}\{w_\beta(x,y)e^{j\omega_\beta t}\},\quad \beta=1,2,3,\ldots \tag{4}$$

which leads to the eigenproblem

$$-\sigma\omega_\beta^2 w_\beta+D\nabla^4 w_\beta=0,\quad \beta=1,2,3,\ldots \tag{5}$$

Here, the boundary conditions presented in Eq. (2) are implied. The functions $w_\beta(x,y)$ are the modeshapes and ω_β are the natural vibration frequencies. The first three modes are zero-frequency modes corresponding to rigid body heave, pitch, and roll and it will be assumed that, in unnormalized form, these will be defined such that

$$w_1(x,y)=1,\quad w_2(x,y)=x,\quad w_3(x,y)=y \tag{6}$$

These and the true vibration modes will be normalized so that $\int_B \sigma w_\beta^2\,dS=1$, $\beta=1,2,3,\ldots$.

Let us now direct our attention to forced time-harmonic motions of the plate and fluid:

$$w(x,y,t)=\sum_{\beta=1}^{N}\mathrm{Re}\{q_\beta w_\beta(x,y)e^{j\omega t}\} \tag{7}$$

The motion of the fluid is governed by the velocity potential $\Phi(\mathbf{r},t)$ which in V satisfies Laplace's equation $\nabla^2\Phi=0$. It can be

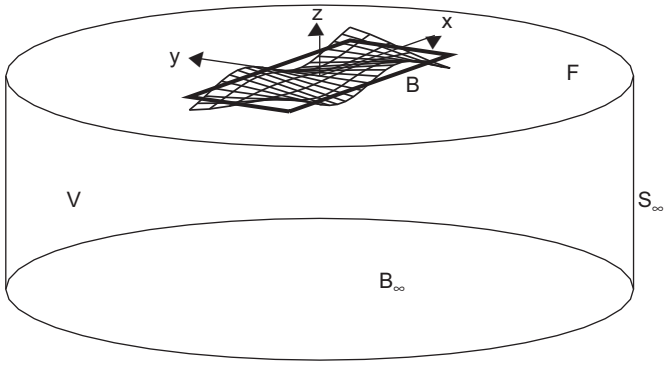

Fig. 1. Fluid domain with floating plate.

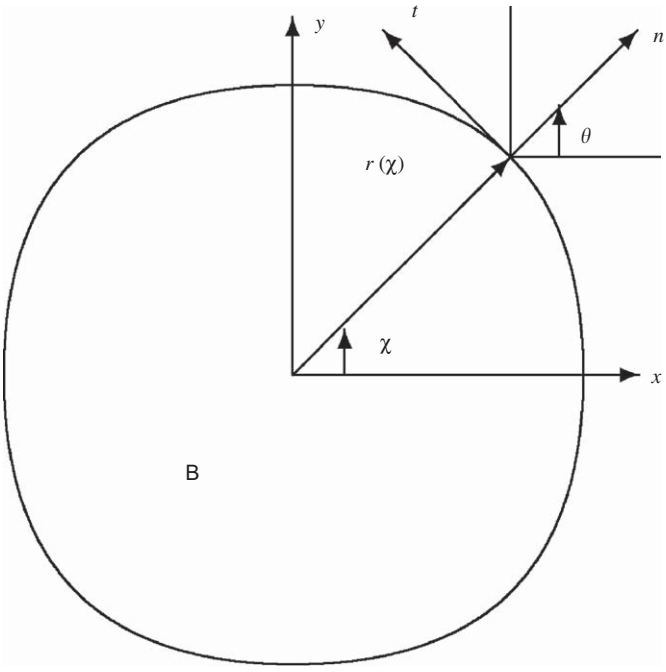

Fig. 2. Plate boundary geometry.

written as

$$\Phi(\mathbf{r},t)=\mathrm{Re}\left\{\left[\zeta(\phi_I(\mathbf{r})+\phi_S(\mathbf{r}))+\sum_{\beta=1}^{N}j\omega q_\beta\phi_\beta(\mathbf{r})\right]e^{j\omega t}\right\} \tag{8}$$

where ζ is the amplitude of an incident plane progressive wave propagating in the positive $x-$direction with time dependence of the form $e^{j\omega t}$. The spatial potential in this case is given by

$$\phi_I=\frac{jg}{\omega}e^{kz}e^{-jk'x} \tag{9}$$

where $k=\omega^2/g$, g is the acceleration due to gravity, and $k'=k\,\mathrm{sgn}(\omega)$.

The radiation potentials $\phi_\beta(\mathbf{r})$ satisfy the following equations:

$$\nabla^2\phi_\beta=0 \text{ in } \mathsf{V} \tag{10}$$

$$\frac{\partial\phi_\beta}{\partial z}=w_\beta \text{ on } \mathsf{B} \tag{11}$$

$$\frac{\partial\phi_\beta}{\partial z}=-k\phi_\beta \text{ on } \mathsf{F} \tag{12}$$

$$\frac{\partial\phi_\beta}{\partial z}=0 \text{ on } \mathsf{B}_\infty \tag{13}$$

$$\frac{\partial\phi_\beta}{\partial r}=-jk\phi_\beta \text{ on } \mathsf{S}_\infty \tag{14}$$

The last of these is recognized as the radiation condition where $r=\sqrt{x^2+y^2}$. The scattered potential ϕ_S satisfies Eqs. (10), (12)–(14), and

$$\frac{\partial\phi_S}{\partial z}=-\frac{\partial\phi_I}{\partial z} \text{ on } \mathsf{B} \tag{15}$$

instead of Eq. (11). Note that Eqs. (8), (11), and (15) ensure that the boundary condition $\partial\Phi/\partial z=\dot{w}(x,y,t)$ is satisfied on B.

Using Bernoulli's equation the linearized fluid pressure is given by

$$p(x,y,t)=-\rho\frac{\partial\Phi}{dt}-\rho gz$$

where ρ is the fluid density. When this and the modal expansion in Eq. (7) are substituted into the motion equation in Eq. (1) and the result is premultiplied by w_α and integrated over B, we arrive at

$$\sum_{\beta=1}^{N}(-\omega^2M_{\alpha\beta}+K_{\alpha\beta})\mathrm{Re}\{q_\beta e^{j\omega t}\}=\mathrm{Re}\{f_\alpha e^{j\omega t}\} \tag{16}$$

where $M_{\alpha\beta}=\int_{\mathsf{B}}\sigma w_\alpha w_\beta\,dS$ and $K_{\alpha\beta}=\int_{\mathsf{B}}w_\alpha D\nabla^4 w_\beta\,dS$. The orthogonality properties of the natural modes are such that $M_{\alpha\beta}=\delta_{\alpha\beta}$ and $K_{\alpha\beta}=\omega_\alpha^2\delta_{\alpha\beta}$.

The (generalized) force coefficient is given by

$$f_\alpha=\sum_{\beta=1}^{N}[-j\omega H_{\alpha\beta}q_\beta-K_{s,\alpha\beta}q_\beta]+\zeta\cdot f_{D\alpha} \tag{17}$$

where $K_{s,\alpha\beta}=\rho g\int_{\mathsf{B}}w_\alpha w_\beta\,dS=(\rho g/\sigma)\delta_{\alpha\beta}$ are the hydrostatic restoring force stiffnesses, the diffraction force coefficients are given by

$$f_{D\alpha}=-j\omega\rho\int_{\mathsf{B}}(\phi_I+\phi_S)w_\alpha\,dS \tag{18}$$

and the radiation impedance is

$$H_{\alpha\beta}=j\omega\rho\int_{\mathsf{B}}\phi_\beta w_\alpha\,dS=j\omega\mu_{\alpha\beta}+\lambda_{\alpha\beta} \tag{19}$$

with

$$\lambda_{\alpha\beta}=-\omega\rho\int_{\mathsf{B}}w_\alpha\mathrm{Im}\phi_\beta\,dS \tag{20}$$

$$\mu_{\alpha\beta}=\rho\int_{\mathsf{B}}w_\alpha\mathrm{Re}\phi_\beta\,dS \tag{21}$$

Here, $\lambda_{\alpha\beta}$ are the damping coefficients and $\mu_{\alpha\beta}$ are the added mass coefficients. It is well known that the damping coefficients are associated with the production of outgoing wave radiation and the degree of energy dissipation for the body is proportional to it (Mei, 1989).

Using Eqs. (16)–(19), the modal coordinates satisfy

$$\sum_{\beta=1}^{N}[-\omega^2(M_{\alpha\beta}+\mu_{\alpha\beta})+j\omega\lambda_{\alpha\beta}+(K_{\alpha\beta}+K_{s,\alpha\beta})]q_\beta=\zeta\cdot f_{D\alpha},\quad \alpha=1,\ldots,N \tag{22}$$

This can be used to determine the q_β which can be substituted in Eq. (7) to determine plate deflection which in turn can be used in Eq. (3) to determine the bending moment amplitudes.

3. Finite element modelling of the plate motion

In this section, we establish the numerical procedures used to determine the vibration mode shapes $w_\alpha(x,y)$ corresponding to three plate shapes: a circular plate, a square plate, and the optimal shape obtained by Damaren (2007). The latter was chosen to maximize the damping coefficient in heave subject to a unit area

Table 1
Optimal Fourier coefficients describing plate boundary.

n	a_n
0	0.8305
1	0.0012
2	−0.1335
3	−0.0044
4	−0.4263
5	0.0064
6	0.2171
7	0.0028
8	0.1631
9	−0.0059
10	−0.1356

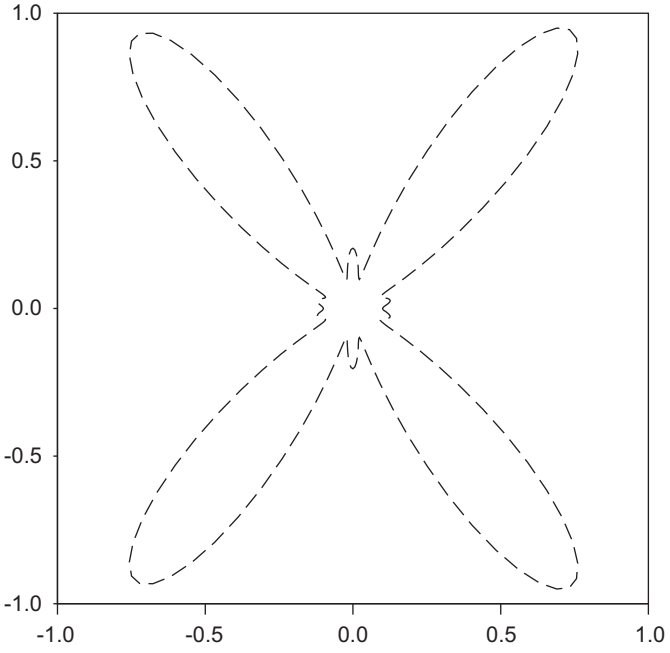

Fig. 3. Optimal floating plate for maximum damping in heave.

constraint ($A = 1\,\mathrm{m}^2$), a perimeter constraint (i.e., $\mathcal{P} \le 10\,\mathrm{m}$), and a minimum dimension constraint (i.e., $r \ge 0.1\,\mathrm{m}$ in polar coordinates). The optimization was performed at a wave number of $k\sqrt{A} = 1.4$.

The shape was parameterized using polar coordinates (refer to Fig. 2):

$$r(\chi) = \frac{a_0}{2} + \sum_{n=1}^{10} a_n \cos n\chi$$

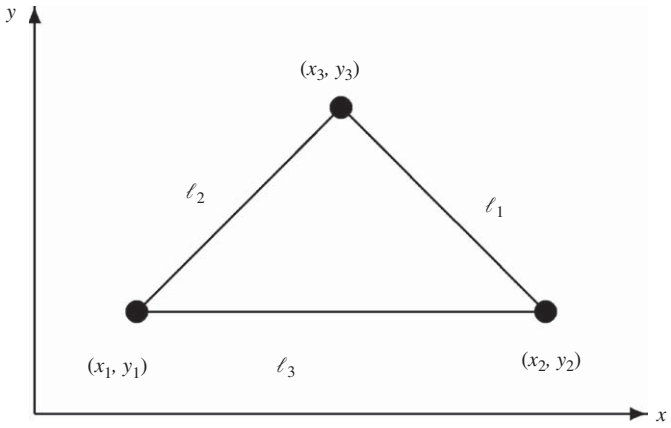

Fig. 4. Triangular finite element.

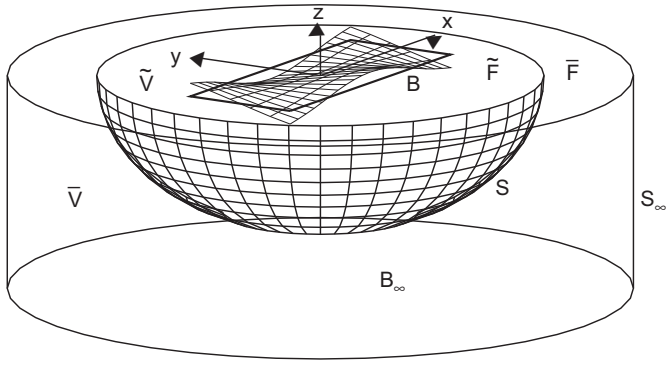

Fig. 5. Discretization for variational formulation.

To be specific, defining $\mathbf{a} = [a_0, \ldots, a_{10}]^T$, the cost function was

$$J(\mathbf{a}) = \frac{\lambda_{1,1}}{\rho\omega} = -\int_{\mathbf{B}(\mathbf{a})} \mathrm{Im}\phi_1 \, dS$$

where ϕ_1 satisfies Eqs. (10)–(14) with $w_1(x,y) = 1$. The area, perimeter, and minimum dimension constraints all represent constraints on the design parameters $\mathbf{a}$. A sequential quadratic programming code (NPSOL) was used to perform a gradient-based optimization. The gradients were calculated using an adjoint-based technique as detailed by Damaren (2007). The optimal coefficients are given in Table 1 and the shape is given in Fig. 3. The multiple lobes on this structure make it suitable for use as a floating airport with multiple runways.

In order to discretize the partial differential equation (PDE) given in Eq. (1), the finite element method is employed. Given the irregular and varied nature of the shapes to be discretized, triangular elements will be employed (Fig. 4).

The trial function used is that developed by Specht (1988) which satisfies the so-called patch test:

$$w(x,y,t) = \sum_{i=1}^{9} d_i(t)\psi_i(x,y) = \boldsymbol{\psi}^T(x,y)\,\mathbf{d}(t) \tag{23}$$

where

$$\begin{aligned}\boldsymbol{\psi}^T = \mathrm{row}\{\psi_i\} = \{&L_1, L_2, L_3, L_1L_2, L_2L_3, L_3L_1,\\ &L_1^2L_2 + \frac{1}{2}L_1L_2L_3[3(1-\mu_3)L_1 - (1+3\mu_3)L_2 + (1+3\mu_3)L_3],\\ &L_2^2L_3 + \frac{1}{2}L_1L_2L_3[3(1-\mu_1)L_2 - (1+3\mu_1)L_3 + (1+3\mu_1)L_1],\\ &L_3^2L_1 + \frac{1}{2}L_1L_2L_3[3(1-\mu_2)L_3 - (1+3\mu_2)L_1 + (1+3\mu_2)L_2]\Big\}\end{aligned}$$

Here,

$$\mu_1 = \frac{\ell_3^2 - \ell_2^2}{\ell_1^2}, \quad \mu_2 = \frac{\ell_1^2 - \ell_3^2}{\ell_2^2}, \quad \mu_3 = \frac{\ell_2^2 - \ell_1^2}{\ell_3^2}$$

where ℓ_1, ℓ_2, and ℓ_3 are the lengths of the triangle sides in Fig. 4. The L_i functions are given by

$$L_i = (a_i + b_i x + c_i y)/(2\Delta), \quad i = 1,2,3, \quad \Delta = \frac{1}{2}\det\begin{bmatrix}1 & x_1 & y_1\\ 1 & x_2 & y_2\\ 1 & x_3 & y_3\end{bmatrix}$$

where

$$a_1 = x_2y_3 - x_3y_2, \quad b_1 = y_2 - y_3, \quad c_1 = x_3 - x_2$$

$$a_2 = x_3y_1 - x_1y_3, \quad b_2 = y_3 - y_1, \quad c_2 = x_1 - x_3$$

$$a_3 = x_1y_2 - x_2y_1, \quad b_3 = y_1 - y_2, \quad c_3 = x_2 - x_1$$

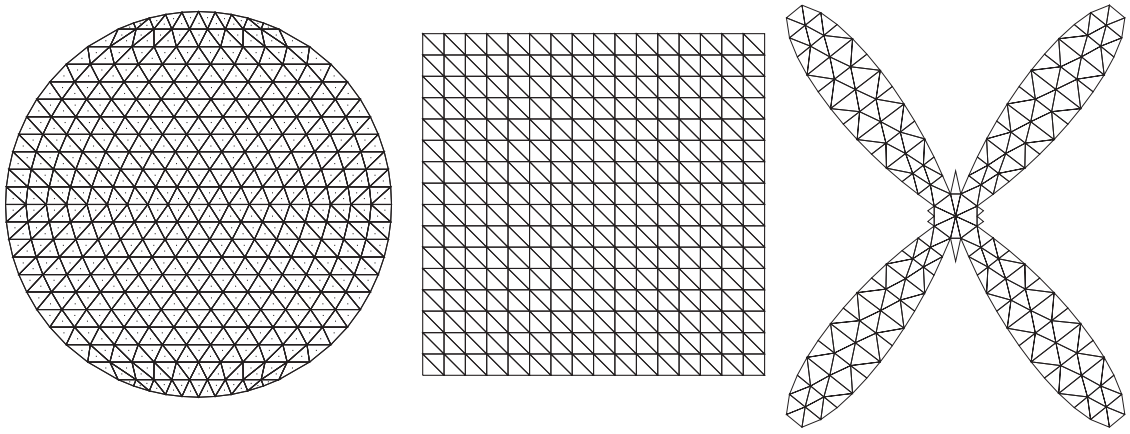

Fig. 6. Finite element meshes.

The nodal degrees of freedom are the deflections $w(x_i, y_i)$ and the slopes $w_{x,i} = \partial w(x_i, y_i)/\partial x$ and $w_{y,i} = \partial w(x_i, y_i)/\partial y$, $i = 1, 2, 3$. If we define

$$\mathbf{q}_e = \mathrm{col}\{w(x_1, y_1), w_{x,1}, w_{y,1}, w(x_2, y_2), w_{x,2}, w_{y,2}, w(x_3, y_3), w_{x,3}, w_{y,3}\} \tag{24}$$

then $\mathbf{d}(t) = \mathbf{A}\mathbf{q}_e(t)$ where $\mathbf{A}$ is selected to that $w(x, y, t)$ and its derivatives as given by Eq. (23) yield the elements of $\mathbf{q}_e$ at the nodes.

The discretized form of the PDE in Eq. (1) takes the form

$$\overline{\mathbf{M}}\ddot{\mathbf{q}} + \overline{\mathbf{K}}\mathbf{q} = \overline{\mathbf{f}} \tag{25}$$

where $\mathbf{q}$ contains the totality of the nodal degrees of freedom and the mass matrix $\overline{\mathbf{M}}$ and stiffness matrix $\overline{\mathbf{K}}$ result from discretizing the kinetic energy and strain energy corresponding to Eq. (1). The discrete form of the eigenproblem in Eq. (5) is

$$-\omega_\alpha^2 \overline{\mathbf{M}}\mathbf{q}_\alpha + \overline{\mathbf{K}}\mathbf{q}_\alpha = \mathbf{0}, \quad \alpha = 1, 2, 3, \ldots \tag{26}$$

The corresponding elemental contributions to the eigenvectors are denoted $\mathbf{q}_{e,\alpha}$ and the modeshapes, described within each

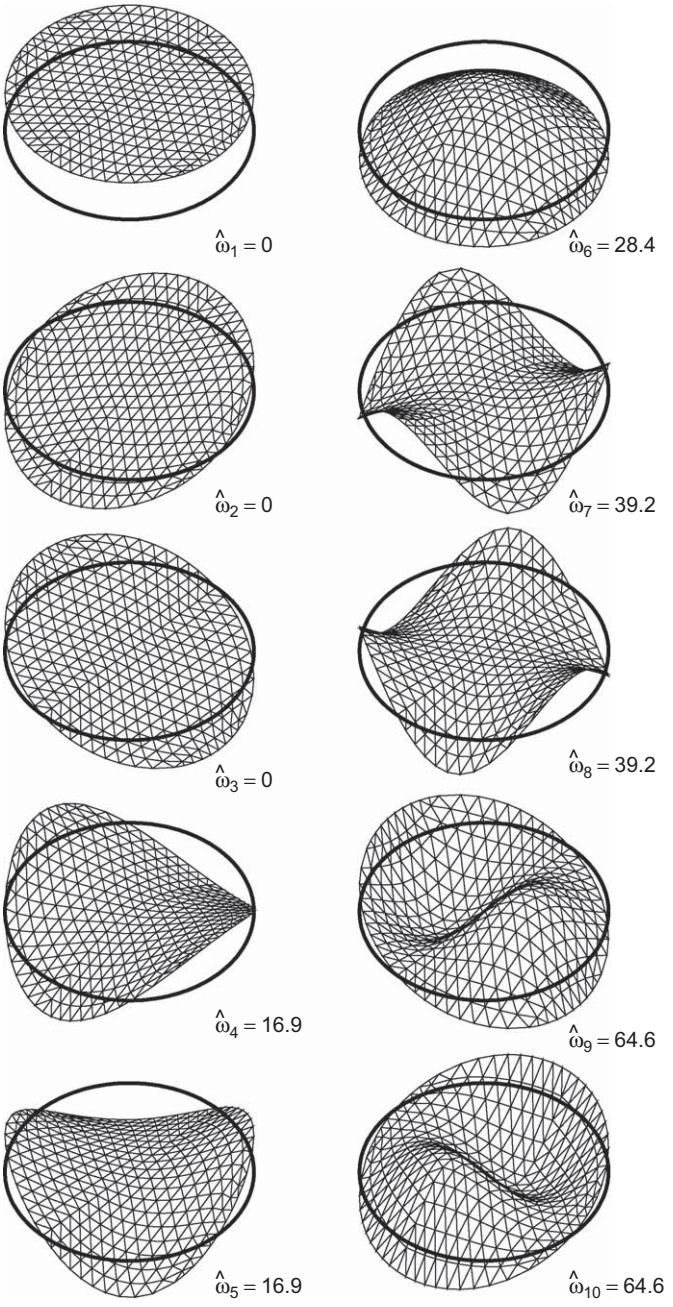

Fig. 7. Modeshapes for the circular plate.

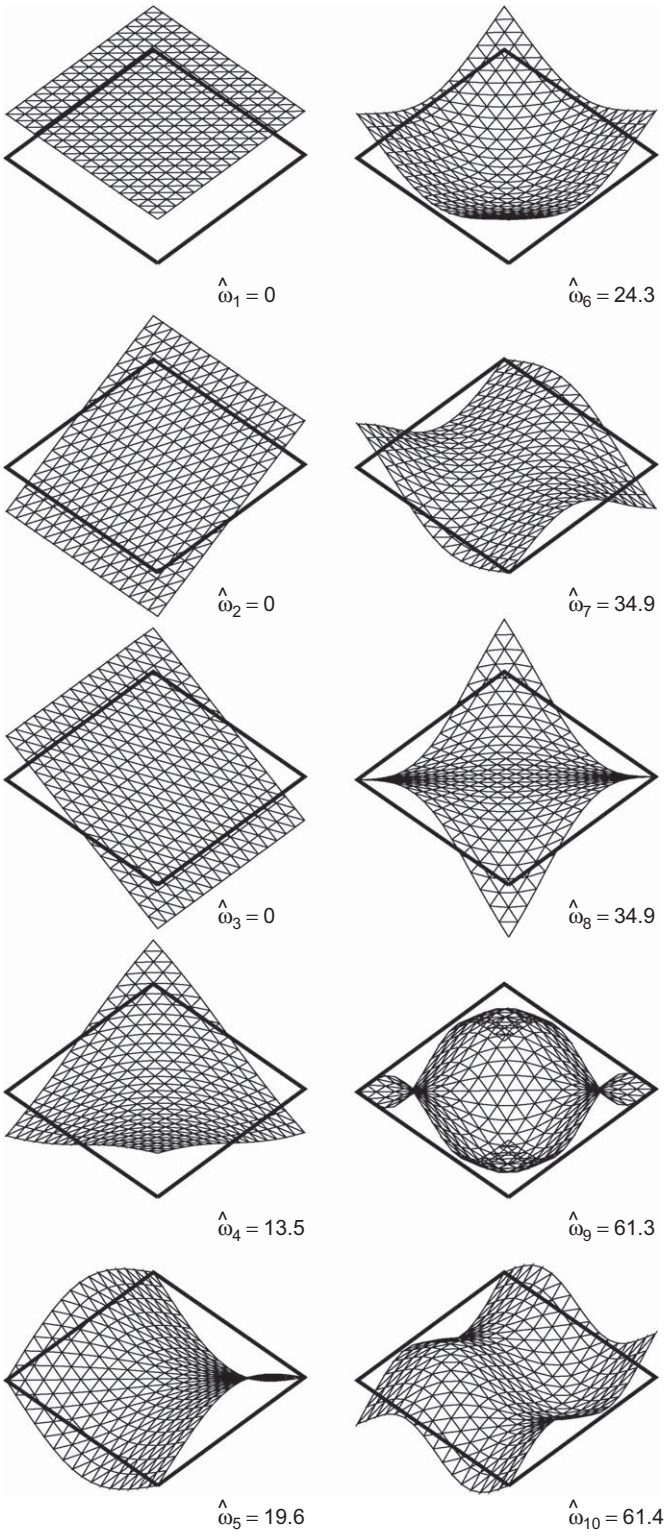

Fig. 8. Modeshapes for the square plate.

element, can be recovered from

$$w_\alpha(x,y) = \boldsymbol{\psi}^T(x,y)\mathbf{A}\mathbf{q}_{e,\alpha}. \tag{27}$$

4. Variational formulation of the radiation and diffraction problems

Let us now examine a computational procedure for determining the solution of the flow problem specified by Eqs. (10)–(14). Consider the geometry in Fig. 5 which was adopted by Damaren (2001) for examining the hydroelastic properties of a rectangular plate. Details of the method are found there but the main ideas are summarized here for completeness. Here, S denotes the surface of a hemisphere of radius a_h which encloses the plate and is centred at the origin. The fluid region $\tilde{\mathsf{V}}$ denotes the interior of S and $\overline{\mathsf{V}}$ denotes its complement in V, i.e., $\overline{\mathsf{V}} \cup \tilde{\mathsf{V}} = \mathsf{V}$. The free surface of $\tilde{\mathsf{V}}$ is $\tilde{\mathsf{F}}$ which is a circular region less the plate surface B. The free surface corresponding to $\overline{\mathsf{V}}$ is denoted by $\overline{\mathsf{F}}$. Hence, $\overline{\mathsf{F}} \cup \tilde{\mathsf{F}} = \mathsf{F}$.

The solution to the flow problem will be constructed using the variational principle of Chen and Mei (Mei, 1989) where the solution $\phi_\beta = \tilde{\phi}_\beta$ in the inner region $\tilde{\mathsf{V}}$ containing the plate is matched on S to an outer solution $\phi_\beta = \overline{\phi}_\beta$ in $\overline{\mathsf{V}}$ which satisfies the radiation condition.

Mei (1989) demonstrates that minimization of the functional

$$\mathcal{K}(\tilde{\phi}_\beta, \overline{\phi}_\beta) = \frac{1}{2}\int_{\tilde{\mathsf{V}}} \boldsymbol{\nabla}\tilde{\phi}_\beta \cdot \boldsymbol{\nabla}\tilde{\phi}_\beta \, dV - \frac{1}{2}k\int_{\tilde{\mathsf{F}}} \tilde{\phi}_\beta^2 \, dS + \int_{\mathsf{S}} \left(\frac{1}{2}\overline{\phi}_\beta - \tilde{\phi}_\beta\right)\frac{\partial\overline{\phi}_\beta}{\partial n} \, dS - \int_{\mathsf{B}} \tilde{\phi}_\beta w_\beta \, dA \tag{28}$$

yields a function $\tilde{\phi}_\beta$ which weakly satisfies Eq. (10) with Eqs. (11) and (12) satisfied as natural boundary conditions. If $\overline{\phi}_\beta$ is selected to exactly satisfy Eqs. (10), (12)–(14), then the following matching conditions are obtained as natural boundary conditions:

$$\tilde{\phi}_\beta(\mathbf{r}) = \overline{\phi}_\beta(\mathbf{r}), \quad \frac{\partial\tilde{\phi}_\beta}{\partial n}(\mathbf{r}) = \frac{\partial\overline{\phi}_\beta}{\partial n}(\mathbf{r}), \quad \mathbf{r} \in \mathsf{S} \tag{29}$$

where n is the outward normal to the hemisphere.

Yu et al. (1978) show that the solution of the diffraction problem $\tilde{\phi}_D = \tilde{\phi}_I + \tilde{\phi}_S$ can be determined by minimizing the following functional:

$$\mathcal{J}(\tilde{\phi}_D, \overline{\phi}_S) = \frac{1}{2}\int_{\tilde{\mathsf{V}}} \boldsymbol{\nabla}\tilde{\phi}_D \cdot \boldsymbol{\nabla}\tilde{\phi}_D \, dV - \frac{1}{2}k\int_{\tilde{\mathsf{F}}} \tilde{\phi}_D^2 \, dS + \int_{\mathsf{S}} \left(\frac{1}{2}\overline{\phi}_S - \tilde{\phi}_D\right)\frac{\partial\overline{\phi}_S}{\partial n} \, dS + \int_{\mathsf{S}} \left(\tilde{\phi}_I\frac{\partial\overline{\phi}_S}{\partial n} - \tilde{\phi}_D\frac{\partial\tilde{\phi}_I}{\partial n}\right) dA \tag{30}$$

This also yields a function $\tilde{\phi}_D$ which weakly satisfies Eq. (10) with Eqs. (12) and (15) satisfied as natural boundary conditions. If $\overline{\phi}_S$ is selected to exactly satisfy Eqs. (10), (12)–(14), then the following matching conditions are obtained as natural boundary conditions:

$$\tilde{\phi}_D(\mathbf{r}) = \overline{\phi}_S(\mathbf{r}) + \tilde{\phi}_I(\mathbf{r}), \quad \frac{\partial\tilde{\phi}_D}{\partial n}(\mathbf{r}) = \frac{\partial\overline{\phi}_S}{\partial n}(\mathbf{r}) + \frac{\partial\tilde{\phi}_I}{\partial n}(\mathbf{r}), \quad \mathbf{r} \in \mathsf{S} \tag{31}$$

Since $\tilde{\phi}$, i.e., $\tilde{\phi}_\beta$ or $\tilde{\phi}_D$, is bounded in $\tilde{\mathsf{V}}$, including at the origin, it is expanded in spherical harmonics as

$$\tilde{\phi}(\mathbf{r}) = \sum_{m=0}^{M_s}\sum_{n=m}^{N_s} A_{nm}\phi_{nm}(\mathbf{r}) + \sum_{m=1}^{M_s}\sum_{n=m}^{N_s} B_{nm}\psi_{nm}(\mathbf{r}) \tag{32}$$

where

$$\phi_{nm}(\mathbf{r}) = \left(\frac{R}{a_h}\right)^n P_n^m(\cos\mu)\cos m\chi, \quad \psi_{nm}(\mathbf{r}) = \left(\frac{R}{a_h}\right)^n P_n^m(\cos\mu)\sin m\chi$$

The spherical coordinates $\{R, \mu, \chi\}$ are chosen such that

$$x = R\sin\mu\cos\chi, \quad y = R\sin\mu\sin\chi, \quad z = -R\cos\mu$$

and P_n^m are the associated Legendre functions as defined by Hulme (1982). On the free surface, $R = r = \sqrt{x^2+y^2}$.

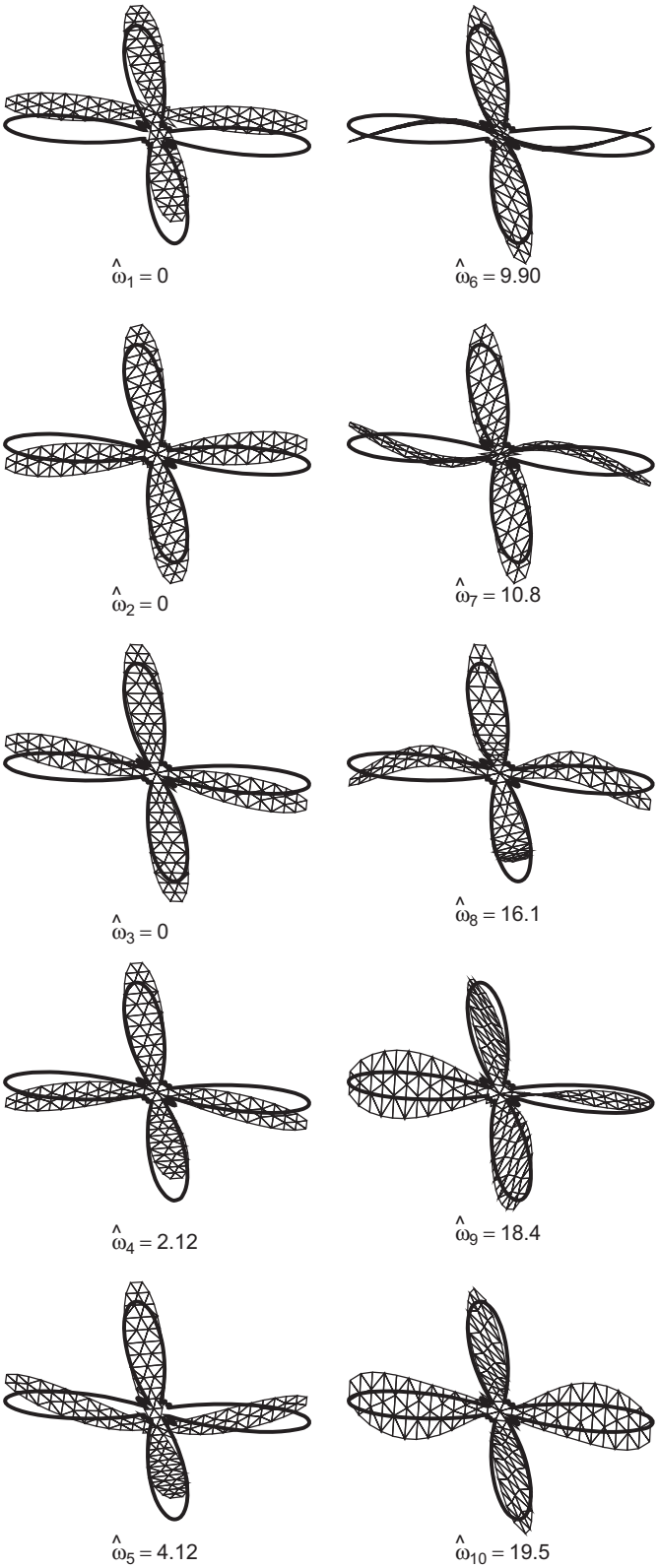

Fig. 9. Modeshapes for the optimal plate.

For the potential exterior to the hemisphere, we express $\overline{\phi}$, i.e., $\overline{\phi}_\beta$ or $\overline{\phi}_S$, using a source distribution on S:

$$\overline{\phi}(\mathbf{r}) = \int_S G(\mathbf{r},\boldsymbol{\xi})\gamma(\boldsymbol{\xi})\, dS_\xi \tag{33}$$

where the source distribution $\gamma(\mathbf{r})$ is selected according to

$$\frac{\partial \overline{\phi}(\mathbf{r})}{\partial n} = -2\pi\gamma(\mathbf{r}) + \int_S \frac{\partial G(\mathbf{r},\boldsymbol{\xi})}{\partial n_r}\gamma(\boldsymbol{\xi})\, dS_\xi \tag{34}$$

The Green's function $G(\mathbf{r},\boldsymbol{\xi})$ satisfies Laplace's equation (except at $\mathbf{r}=\boldsymbol{\xi}$), the free surface, bottom, and radiation conditions and is described in Damaren (2007).

The discretization of $\mathcal{K}(\tilde{\phi}_\beta, \overline{\phi}_\beta)$ and $\mathcal{J}(\tilde{\phi}_D, \overline{\phi}_S)$ and subsequent minimization with respect to the A_{nm}, B_{nm}, and the source strengths comprising $\gamma(\mathbf{r})$ is straightforward. The integrals corresponding to the first term in Eqs. (28) and (30) can be done analytically (Damaren, 2001) and the second and third terms are simple when the source distribution, the potential $\overline{\phi}_\beta$ or $\overline{\phi}_S$ and their normal derivatives, and the Green's function are taken to be

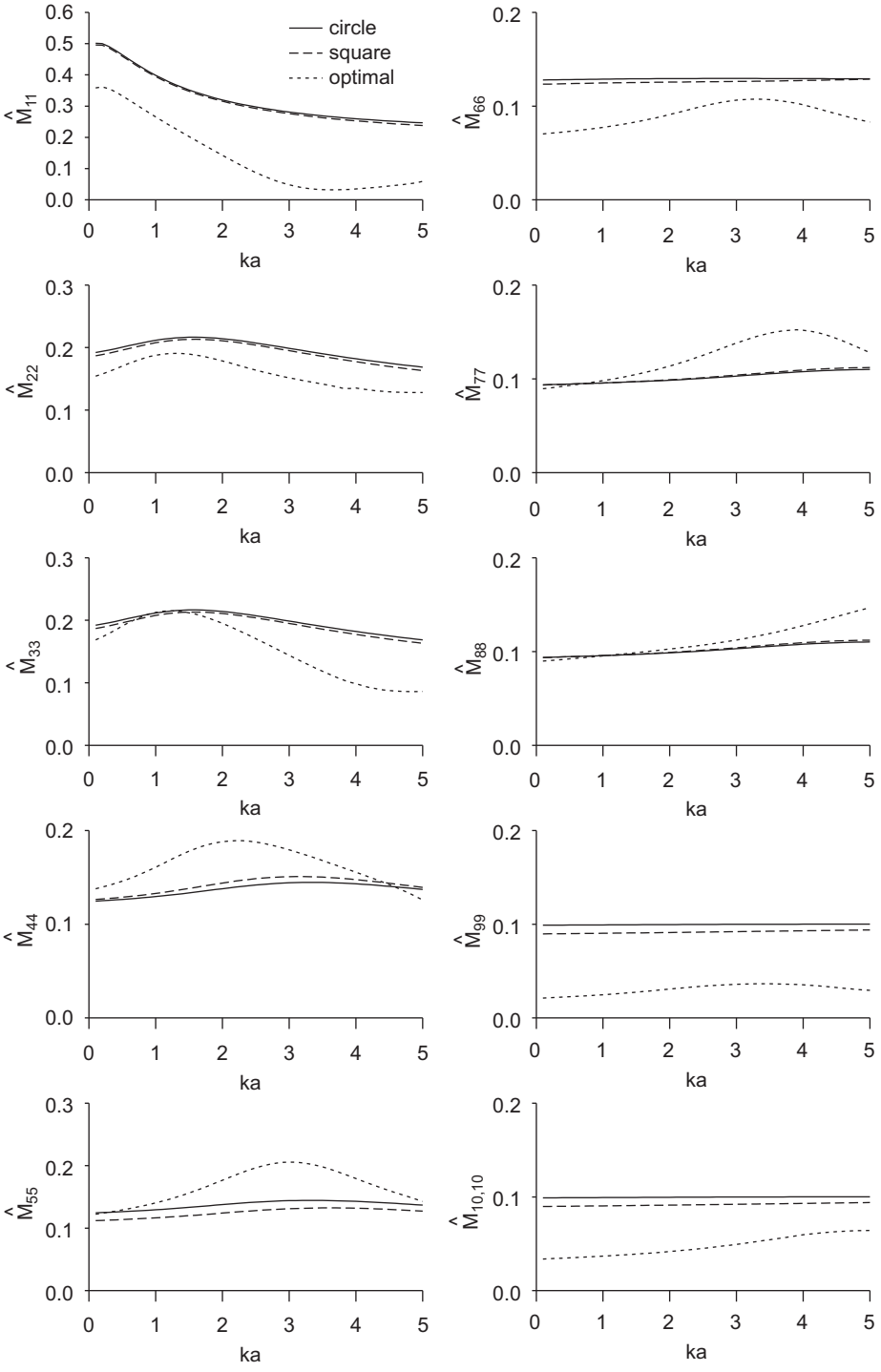

Fig. 10. Added mass coefficients for the circular, square, and optimal plates.

piecewise constant on S. For the last term in Eq. (28), the integral involves products of spherical harmonics and the finite element trial function in Eq. (23). These are performed using 13-point Gauss quadrature for triangles (Bathe, 1995). A similar technique is used to calculate the added mass, damping, and diffraction force coefficients.

5. Numerical example

The finite element meshes used for each shape are given in Fig. 6. The vibration mode shapes obtained are given in Figs. 7–9 along with the corresponding natural frequencies where we have nondimensionalized according to $\hat{\omega}_\alpha^2 = (\sigma A^2/D)\omega_\alpha^2$. Note that the first three modes in each case are the zero frequency modes corresponding to heave, pitch, and roll.

Given the area A, let us define $a = \sqrt{A}$. The hydrodynamic coefficients introduced in Eqs. (18)–(21) will be nondimensionalized according to

$$\hat{M}_{\alpha\alpha} = \frac{m}{\rho a^3}\mu_{\alpha\alpha}$$

$$\hat{D}_{\alpha\alpha} = \frac{m}{\omega\rho a^3}\lambda_{\alpha\alpha}$$

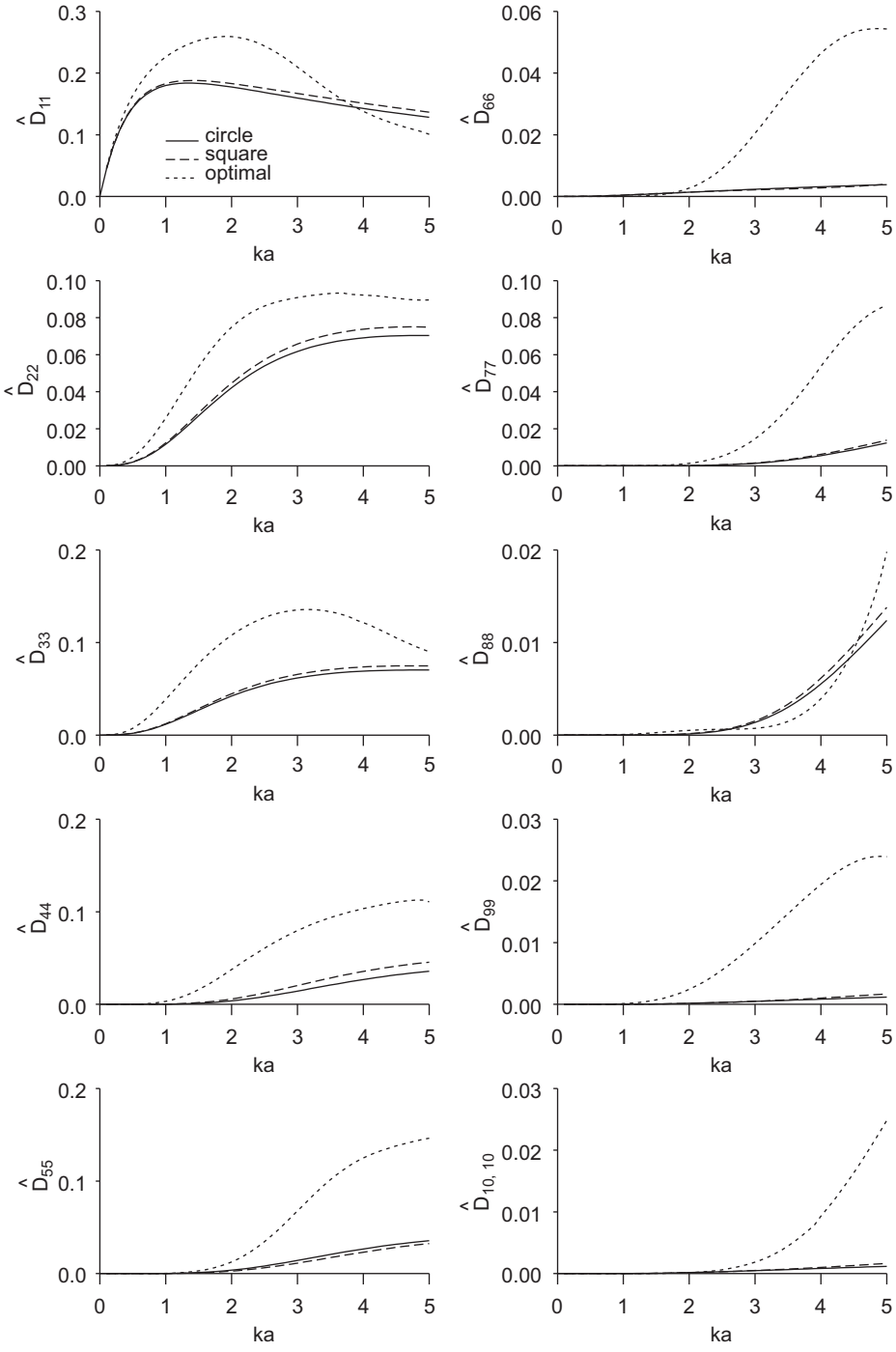

Fig. 11. Damping coefficients for the circular, square, and optimal plates.

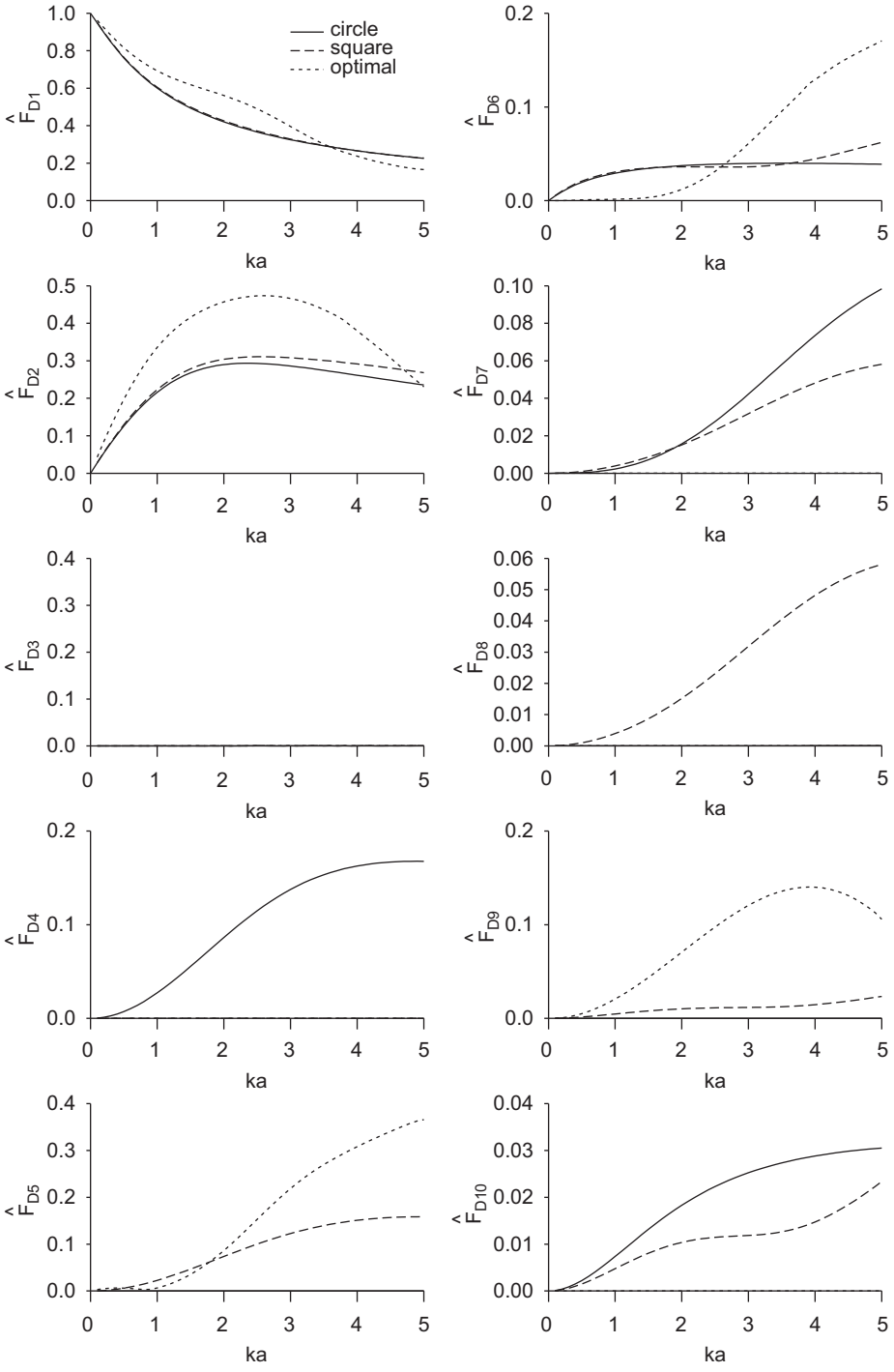

Fig. 12. Diffraction force coefficients for the circular, square, and optimal plates.

$$\hat{F}_{D\alpha} = \frac{m}{\rho g A}|f_{D\alpha}|$$

where m is the mass of the plate. These quantities are presented as a function of nondimensionalized wave number ka in Figs. 10–12 for each of the three shapes. It is very clear that the damping coefficient for the optimal shape is substantially greater than the baseline circular and square plates although the optimal plate shape was optimized for rigid heave at only one wave number. The diffraction forces for the optimal plate are increased over the baselines for modes 1, 2, 5, 6, and 9.

At each frequency, the modal coordinates can be determined from Eq. (22) which can be substituted into Eq. (7) to determine the amplitude of the plate deflection. Substituting from Eq. (7) into Eq. (3) yields the amplitude of the bending moments. We shall nondimensionalize these quantities according to

$$\hat{W} = \frac{|w(0,0,t)|_{\max}}{\zeta}$$

$$\hat{M}_x = \frac{|M_x(0,0,t)|_{\max} A}{D\zeta}$$

$$\hat{M}_y = \frac{|M_y(0,0,t)|_{\max} A}{D\zeta}$$

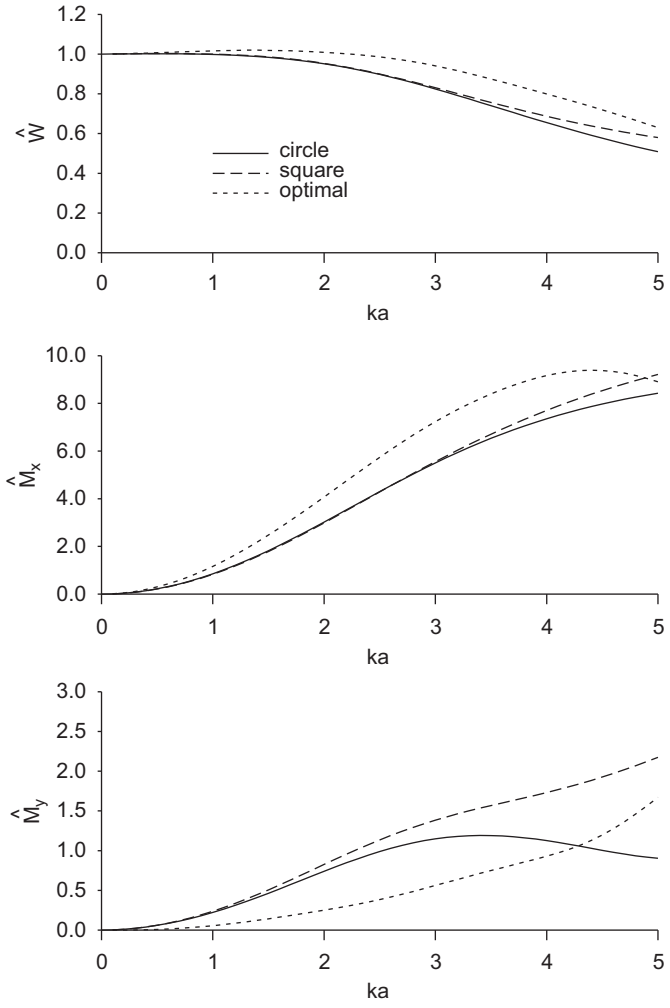

Fig. 13. Plate deflection and bending moment amplitudes.

Here, $|(\cdot)|_{\max}$ denotes the amplitude of the corresponding expressions in Eqs. (3) and (7) which exhibit time dependence of the form $e^{j\omega t}$. Note that these quantities are evaluated at the origin (mass centre) of each of plate shapes. It is understood that not all modes will contribute in this case, but it is the only location that can be used for a meaningful comparison between the disparate shapes.

The following nondimensional parameters specify the mass and stiffness properties of the plate: $D/(\rho A^2 g) = 0.001$ and $\sigma/(\rho a) = 0.01$. For this case, the deflection and bending moments are plotted against nondimensional wave number in Fig. 13. It is interesting to note that, although the optimal plate exhibited considerably greater radiation damping than the other shapes, it leads to greater plate deflection and bending moment about the $x-$axis. This is somewhat surprising but not completely unexpected given the increases in the diffraction forces for the optimal plate. The bending moment about the $y-$axis is reduced somewhat.

6. Conclusions

This paper has examined the hydroelastic properties of the vibration modes of a thin plate floating on the surface of an incompressible, inviscid, irrotational ocean of infinite extent. Circular and square plates have been examined along with a plate whose shape has been optimized for maximum radiation damping for rigid heave motions at one wave number. The results demonstrate that, although structural flexibility was not taken into account in the optimization, the vibration modes exhibit large damping coefficients compared to the circular and square cases. This is expected to lead to increased damping of transient responses such as those produced by landing aircraft on a floating runway. However, the steady-state plate deflection in response to incident waves actually increases for the optimal plate due to an increase in the magnitude of the diffraction forces. A similar trend was observed for the bending moment about the $x-$axis but that about the $y-$axis was moderately reduced.

References

Andrianov, A.I., Hermans, A.J., 2005. Hydroelasticity of a circular plate on water of finite or infinite depth. Journal of Fluids and Structures 20, 719–733.
Bathe, K.J., 1995. Finite Element Procedures. Prentice-Hall, Englewood Cliffs, NJ.
Chen, H.S., Mei, C.C., 1974. Oscillations and wave forces in a man-made harbour in the open sea. In: Proceedings of the 10th Symposium on Naval Research, Office of Naval Research, pp. 573–594.
Damaren, C.J., 2001. The hydrodynamics of thin floating plates. Ocean Engineering 28, 1145–1170.
Damaren, C.J., 2007. Hydrodynamic shape optimization of thin floating plates. Ocean Engineering 34, 2231–2239.
Ertekin, R.C., Kim, J.W., 1999. Hydroelastic response of a floating, mat-type structure in oblique, shallow-water waves. Journal of Ship Research 43, 241–254.
Hulme, A., 1982. The wave forces acting on a floating hemisphere undergoing forced periodic oscillations. Journal of Fluid Mechanics 121, 443–463.
Mei, C.C., 1989. The Applied Dynamics of Ocean Surface Waves, second ed. World Scientific, Singapore.
Riggs, H.R., Suzuki, H., Ertekin, R.C., Kim, J.W., Iijmae, K., 2008. Comparison of hydroelastic computer codes based on the ISSC VLFS benchmark. Ocean Engineering 35, 589–597.
Specht, B., 1988. Modified shape functions for the three-node plate bending element passing the patch test. International Journal for Numerical Methods in Engineering 26, 705–715.
Watanabe, E., Utsunomiya, T., Wang, C.M., 2004. Hydroelastic analysis of pontoon-type VLFS: a literature survey. Engineering Structures 26, 245–256.
Watanabe, E., Utsunomiya, T., Wang, C.M., Hang, L.T.H., 2006. Benchmark hydroelastic responses of a circular VLFS under wave action. Engineering Structures 28, 423–430.
Xia, D., Ertekin, R.C., Kim, J.W., 2008. Fluid-structure interaction between a two-dimensional mat-type VLFS and solitary waves by the Green–Naghdi theory. Journal of Fluids and Structures 24, 527–540.